Acta Cryst. (1991). B**47**, 660–672

The Electron-Density Distribution in $KTiOPO_4$

BY NIELS K. HANSEN, JEAN PROTAS AND GÉRARD MARNIER

Laboratoire de Minéralogie, Cristallographie et Physique Infrarouge, UA CNRS 809, *Université de Nancy* I, *BP* 239, *F*-54506 *Vandoeuvre-les-Nancy CEDEX, France*

(*Received* 10 *November* 1990; *accepted* 4 *April* 1991)

Abstract

A detailed account of X-ray diffraction measurements on single crystals of $KTiOPO_4$ (potassium titanyl phosphate) is given. The experiments were carried out at room temperature and the data were used for the analysis of the electron-deformation density. We have been confronted with difficulties in obtaining a correct description of the electron density owing to the noncentrosymmetry of the crystal structure and the probable anharmonic thermal motion or local disorder of the potassium ions. The electron density indicates the presence of a strong covalent bond between Ti^{4+} and O^{2-} ions. The possibility of relating the electron density to the high second-order electronic electric susceptibility of $KTiOPO_4$ has previously been discussed by Hansen, Protas & Marnier [*C. R. Acad. Sci. Ser. B* (1988), **307**, 475–478]. Crystal data: orthorhombic, $Pna2_1$, a = 12·8209 (9), b = 6·4052 (6), c = 10·5932 (9) Å, V = 869·9 Å^3, Z = 8, $R(F)$ = 1·86% for 5053 reflections.

Introduction

$KTiOPO_4$ (KTP) is a compound with large second-order electronic dielectric constants (Zumsteg, Bierlein & Gier, 1976), and is, because of its low thermal expansion coefficients and the slow variation of its optical constants with temperature, very favourable for use as a 'second-harmonic generator' of near-infrared laser light. In a recent publication (Hansen, Protas & Marnier, 1988) the relations between the crystal structure of KTP, the electron density around the titanium ions and the optical properties have been discussed. In the present paper we give a detailed account of the analysis of the X-ray diffraction data in terms of the electron-density distribution in KTP.

The crystal structure of KTP was first determined by Tordjman, Masse & Guitel (1974). An extensive review of the crystal structure and physico-chemical properties of KTP and isostructural compounds has been published recently by Stucky, Phillips & Gier (1989). Thomas, Glazer & Watts (1990) reanalyzed the structure and compared it to that of $KSnOPO_4$.

0108-7681/91/050660-13$03.00

Voloshina, Gerr, Antipin, Tsirel'son, Pavlova, Struchkov, Ozerov & Rez (1985) carried out an X-ray diffraction study of the electron-density distribution in order to determine the second-order polarizabilities of KTP. They intended to use a so-called bond-charge model (BCM) originally proposed by Levine (1973) and modified by Tsirel'son, Korol'kova & Ozerov (1984) who have successfully applied the model to calculate the nonlinear susceptibility of lithium formate monohydrate. The basic idea is that each polar bond with a partial covalent character contributes to the second-order electronic polarizability. The most pronounced deformation-density peaks observed for KTP by Voloshina *et al.* (1985) are in the P—O bonds of the phosphate groups. As we have shown (Hansen, Protas & Marnier, 1988), the high nonlinear polarizability of KTP cannot be explained at all by the phosphate contributions.

The outline of our presentation is as follows. Details of the experiment are given in the first sections in which some of the basic problems in the analysis of the data before examining the resulting electron-density functions are discussed. One difficulty is that KTP crystals have quite a high degree of perfection and as a consequence secondary extinction is quite strong. Furthermore, it appeared that this effect is anisotropic which makes handling the data more cumbersome. Thus, to correct for anisotropic extinction, equivalent reflections cannot be averaged at an early stage of the structural and electron-density refinements. During the refinements it was also realized that the total electron density around the potassium sites is poorly described by harmonically vibrating K^+ ions, and that deficiencies in the model for these ions affect the charge-density maps in other parts of space too. This is contrary to observations for centrosymmetric structures. Several models have been tried, but it will not be possible to give all the details here. We have therefore carefully analyzed the reliability of our results. Another important problem which we have been facing is that for this type of compound some of the electrons may be quite delocalized, and thus hardly contribute to the Bragg intensities, except for the very lowest order

reflections. Following this discussion the final model and the corresponding electron-density distributions are presented. The most important result is the detection of strong interactions between titanium and oxygen ions.

Experimental

KTP crystals were grown by a flux method at a temperature below the ferroelectric phase transition (Marnier, 1988). The sample used was a small crystal of KTP ground into a sphere (diameter 0·23 mm). Two series of measurements were carried out, both at room temperature. The step-scanned intensity profiles were collected in the ω–2θ scan mode on a Nonius CAD-4 diffractometer using monochromatized Ag $K\alpha$ radiation (graphite 002, θ_M = 4·80°, λ = 0·56087 Å). The space group is $Pna2_1$ with $Z = 8$. The unit-cell dimensions were determined from the centring of 22 reflections with θ values between 21 and 28°: a = 12·8209 (9), b = 6·4052 (6), c = 10·5932 (9) Å; the angles were found to be equal to 90° within a random error of 0·01°.

In the first experiment one octant of reflections was collected (h, k, $l \geq 0$), $\sin\theta/\lambda < 0{\cdot}9$ Å^{-1} (θ_{max} = 30°). The scan parameters were width of scan (0·60 + 0·45tanθ)° and horizontal detector aperture (1·65 + 4·8tanθ) mm. The scan speed was determined by a prescan; it varied from 0·63 to 2·75° min^{-1} with the maximum time spent on one profile of 2 min. The raw data set consisted of 2674 reflections of which 2613 were retained after the data reduction.

In the second set, two octants of data (hkl, $hk\bar{l}$), $\sin\theta/\lambda < 1{\cdot}15$ Å^{-1} ($\theta_{max} = 40°$) were collected. The scan parameters were width of scan (0·70 + 0·45tanθ)° and horizontal detector aperture (1·85 + 3·10tanθ) mm. The scan speed was determined by a prescan; it varied from 0·37 to 3·3° min^{-1} with the maximum time spent on one profile of 3 min. The raw data consisted of 11 549 Bragg intensities which after a first data reduction were limited to 9526 reflections, $0 \leq h \leq 29$, $0 \leq k \leq 14$, $-24 \leq l \leq 24$, having $I > 3\sigma(I)$. The precision of this data set was about twice as good as for the less extended set.

For both sets three intensity reference reflections (040, 800, 203) were measured every 3 h and the orientation matrix was checked every 100 reflections. The reference reflections showed random variations of less than half a per cent. The counts were automatically corrected for coincidence loss and strong reflections were measured with a filter. For the peak integration, background subtraction, Lorentz and polarization corrections a program system written by Blessing (1987) was used. The uniqueness of these programs is that an analytical fit of the reflection-profile widths is made for the strongest reflections and subsequently applied to the full data set, but peak positions are determined from the individual rocking curves. Reflections for which $I < 3\sigma(I)$ were rejected. This rejection is justified by the fact that the profile analysis seemed to over estimate the intensities of the weak Bragg reflections; we shall return to this point when discussing the least-squares refinements of the data (see for example Fig. 7). The absorption correction was neglected (μ = 16·5 cm^{-1}, $\mu R = 0{\cdot}18$) since its variation with the scattering angle was less than half a per cent.

Table 1. *Study of enantiomorphs*

Free-atom refinements of the 4529 (N_{obs}) high-order reflections ($\sin\theta/\lambda > 0{\cdot}9$ Å^{-1}) in two octants. N_{var} is the number of parameters refined.

	Enan I $\eta = 1$	Enan II $\eta = 1$	η refinement $\eta = -0{\cdot}08$
N_{var}	144	144	145
$R(F^2)$ (%)	4·65	4·54	4·45
$wR(F^2)$ (%)	5·84	5·73	5·63
G.o.f.	1·308	1·286	1·263

Averaging of the data sets

The X-ray structure factors for a pair of Bragg reflections, hkl and $hk\bar{l}$, are different when taking into account the anomalous dispersion, but in the present case this effect is very weak. It is assumed that the amplitudes f' and f'' are independent of the scattering angle; we used the values tabulated by Sasaki (1984). For titanium, which is the strongest anomalous scatterer in KTP, the contribution of f' for the highest-order reflections in the data set amounts to about 3% and the change in phase angles of the atomic scattering factor due to f'' is about 2·5°. Comparison of the error sums for the high-order refinements ($\sin\theta/\lambda > 0{\cdot}97$ Å^{-1}) showed hardly any differences between the two enantiomorphs (Table 1). Optimizing the values of f' [for all atoms they are multiplied by a common factor η (Rogers, 1981)] by a full-matrix least-squares refinement including structural parameters and the scale factor, and using the high-order data led to $\eta = -0{\cdot}08$ (8). Comparison of the measured intensities

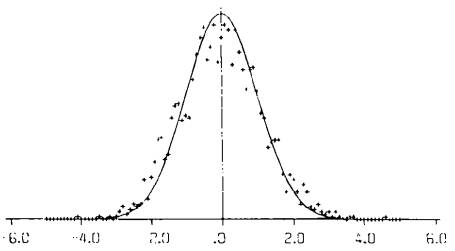

Fig. 1. Distribution of the normalized deviations $\Delta = (I_{hkl} - I_{hk\bar{l}})/\sigma$ (crosses) compared to a normalized Gaussian (continuous curve).

I_{hkl} and $I_{hk\bar{l}}$ showed a good agreement: the observed distribution of the normalized deviations, $(I_{hkl} - I_{hk\bar{l}})/\sigma$, is only slightly broader than a Gaussian (Fig. 1) as is also indicated by their root-mean-square value of 1·16. We cannot explain why the η refinement does not predict unambiguously the polarity of the crystal. All optical measurements on crystals grown in the laboratory confirm that they are single-domain crystals and the crystals ground into spheres do show strong pyroelectric behaviour.

For the strongest low-order reflections, differences between the intensities of hkl and $hk\bar{l}$ reflections amounted to 8%. As the absorption was weak ($A \simeq 0{\cdot}85$), these differences cannot be explained by undetected deviations from the spherical shape of the crystal, but they may rather be attributed to secondary anisotropic extinction. Including secondary anisotropic extinction in the refined models subsequently reduced the differences to at most 3·5% for the Friedel pairs. Nevertheless, the agreement between the calculated structure factors (multipoles included) and the observations were not completely satisfactory: for 40 reflections with $y_{ext} < 0{\cdot}8$ (the measured intensity $I_m = y_{ext} I_{kin}$, where I_{kin} is the kinematical value of the integrated Bragg intensity), 15 had deviates, $F_{obs} - F_{calc}$, larger than five standard deviations; for the full data set there were only 70 reflections, mostly at low values of $\sin\theta/\lambda$, showing a very poor fit. We therefore decided to exclude 43 strongly extinction-affected reflections (24 unique reflections) and subsequently to treat the extinction as isotropic.

The intensities of the reflections hkl and $hk\bar{l}$ were then averaged. For the obtained data set, the root-mean-square value of $(I_{hkl} - I_{hk\bar{l}})/\sigma$ was 1·12 and the deviations did not show any systematic variation with $\sin\theta/\lambda$ or $|F|$. These data (I_{88}) were then averaged with the previously measured set (I_{86}). When the standard deviations for the final data were modified according to:

$$\sigma^2(I) = \sigma^2_{est} + \alpha^2 I^2; \quad \alpha = 0{\cdot}01$$

the distribution of $(I_{88} - I_{86})/\sigma$ was close to a normalized Gaussian. Only seven reflection pairs had deviations above four standard deviations and were eliminated. The results presented in the following paragraphs are from the analysis of this data set consisting of 5053 independent reflections.

Description of the electron-density model

A modified version of the multipole least-squares method refinement program *MOLLY* (Hansen & Coppens, 1978) was used throughout. In addition to a scale factor and the conventional atomic parameters (positions and harmonic anisotropic vibrations), the parameters of various secondary-extinction models (Becker & Coppens, 1974) and a number of atomic density deformation parameters can be refined. The electron density of an atom is described by an expansion of atom-centred functions:

For titanium:

$$\rho_{Ti}(\mathbf{r}) = \rho_{core}(r) + P_{3d}\kappa^3\rho_{3d}(\kappa r) + P_{4s}\rho_{4s}(r) + \sum_{l=1}^{4} \kappa'^3 R_l(\kappa' r) \sum_{m=-l}^{l} P_{lm} y_{lm}(\mathbf{r}/r) \quad (1a)$$

For the other atoms:

$$\rho_{atom}(\mathbf{r}) = \rho_{core}(r) + P_{val}\kappa^3\rho_{val}(\kappa r) + \sum_{l=1}^{4} \kappa'^3 R_l(\kappa' r) \sum_{m=-l}^{l} P_{lm} y_{lm}(\mathbf{r}/r) \quad (1b)$$

where ρ_{core} and ρ_{val}, ρ_{3d} and ρ_{4s} are spherical Hartree–Fock core and valence densities and y_{lm} represents spherical harmonic functions in real form. Radial functions of the form $R_l(r) = Nr^{n_l}\exp(-\zeta r)$ were selected where N is a normalization factor, $n_l = 2, 2, 3$ for the oxygen atoms [hexadecapoles ($l = 4$) were not included for oxygen in the final refinements since they did not significantly improve the fit to the data], $n_l = 4, 4, 6, 8$ for the phosphorus atoms and $n_l = 4, 4, 4, 4$ for $l = 1, 2, 3, 4$ for titanium. It was initially assumed that the potassium could be described by the density of the free monovalent ion, but at a later stage it was found that a highly significant improvement of the fit was obtained by adding a set of very localized multipolar functions [$1 \le l \le 4$, $n_l = 6$, $\zeta = 13{\cdot}6$ Bohr^{-1} (1 Bohr^{-1} = 1·890 Å^{-1}) centred on these ions:

$$\rho_{ion}(\mathbf{r}) = \rho_{K\cdot}(r) + \sum_{l=1}^{4} \kappa'^3 R_l(\kappa' r) \sum_{m=-l}^{l} P_{lm} y_{lm}(\mathbf{r}/r).$$

The core-scattering factors, f_{core}, are taken from *International Tables for X-ray Crystallography* (1974, Vol. IV). The anomalous-scattering amplitudes, which were added to f_{core}, were taken from Sasaki (1984); they are supposed to be independent of the scattering angle. The valence-scattering factors corresponding to ρ_{val} were computed by *MOLLY* from the atomic wavefunctions by Clementi & Roetti (1974). By putting all P_{lm} equal to zero, P_{val} equal to the number of valence electrons of the neutral atom and κ equal to one, formulae (1*a*) and (1*b*) give the density of a free atom.

In the refinements of the electron density the number of parameters was limited by several constraints: the total valence population corresponds to an electrically neutral unit cell; the two crystallographically independent phosphate ions are assumed to have identical deformations, close to tetrahedral symmetry; furthermore, it was thought that the P—O bonds have approximate cylindrical symmetry.

The phosphorus deformation was described by the octopoles y_{30} and y_{33+} and the hexadecapoles y_{40} and y_{43+} (the local z axis was parallel to a P—O bond and the x axis was in the plane through two P—O bonds). All the oxygen atoms in the phosphate groups had identical deformations and only the functions y_{l0} with $l \leq 3$ were used (the z axis was parallel to the P—O bond). Releasing this constraint did not improve the fit significantly. The κ, κ' values were constrained such that there were five sets in the final model: one set for the titanium ions, one for the oxotitanium O^{2-}, one for the phosphorus atoms, one for the phosphate-oxygen atoms and a set for the K^+ ions.

Refining the κ' values of the oxygen atoms led to very diffuse multipole functions and only to minor improvements of fit. Therefore, it was decided to fix the oxygen κ' values at $\kappa'\zeta(O^{2-}) = 2{\cdot}5$ and $\kappa'\zeta$(O phosphate) = 4·0 Bohr^{-1}, corresponding to valence-density distributions which are more diffuse than those observed for organic molecules. Also for the titanium ions refinement of κ' led to very small values, *i.e.* the functions peaked at distances close to the titanium–oxygen bond lengths. It was therefore decided to fix $\kappa'\zeta$(Ti) = 5·4 Bohr^{-1}, a value reproducing reasonably well the density of a titanium 3*d* orbital. The 4*s* orbitals of the free potassium and titanium atoms are so extended in space that they do not have any meaning for the bound ions, and they contribute only to the very lowest order Bragg reflections. Furthermore, refining the 4*s* populations of both of these atom species leads to very large correlations between the valence populations, and even to meaningless results such as a negative number of valence electrons on the potassium ions. Thus, in consequence, the valence population of the K^+ ions was kept equal to zero, which is also a physically realistic hypothesis. It was then possible to refine the titanium 4*s* population parameter. Its value must be interpreted with great circumspection for the above-mentioned reasons, but also because its standard deviation is large ($\simeq 0{\cdot}3$ e, see Table 5), its value being mainly determined by the valence population of the other atoms in conjunction with the electroneutrality constraint. It is nevertheless important to include some diffuse density function in the model in order to allow for a variation in the total number of localized valence electrons.

Electron-density maps (definitions)

The residual density map is calculated by a Fourier synthesis according to

$$\Delta\rho_{\rm res}(\mathbf{r}) = \tfrac{1}{V}\sum_{\mathbf{H}}[|F_{\rm obs}(\mathbf{H})| - |F_{\rm mult}(\mathbf{H})|] \times \exp(i\alpha_M)\exp(-2\pi i\mathbf{H}.\mathbf{r}), \quad (2)$$

and the dynamic deformation-density (X–M map) by

$$\Delta\rho_{\rm dyn}(\mathbf{r}) = \tfrac{1}{V}\sum_{\mathbf{H}}[|F_{\rm obs}(\mathbf{H})|\exp(i\alpha_M) - F_{\rm FA}(\mathbf{H})] \times \exp(-2\pi i\mathbf{H}.\mathbf{r}). \quad (3)$$

α_M is the phase of the structure factor obtained from the converged multipole model. $F_{\rm mult}$ is the structure factor corresponding to the multiple model and $F_{\rm FA}$ the superposition of free-atom densities using the structural parameters of the multipole refinement. The observed structure-factor amplitudes have been brought onto an absolute scale and corrected for secondary extinction using the parameters resulting from the converged multipole refinement.

It is stressed that the X–M map ($\Delta\rho_{\rm dyn}$) mainly depends on the multipole model through the calculated structure-factor phases, α_M. This is probably the closest we can get to a minimal bias model-independent representation of the electron density for a noncentrosymmetric structure.

Static deformation-density maps are calculated directly from the equations (1*a*) and (1*b*) by adding the aspherical pseudo-atom density functions for a cluster of atoms, and from this the electron densities of the free atoms are subtracted. There is no Fourier synthesis involved in this procedure so this map does not suffer explicitly from series-termination effects, or unobserved or rejected reflection contributions.

Description of the crystal structure

In the present context we are mainly interested in the titanium environment. The titanium ions have distorted octahedral coordinations, each being surrounded by four phosphate groups and two oxygen ions (formal charge of −2). Each titanium ion has a short bond to an O^{2-} ion (~ 1·74 Å). For the Ti(1) octahedron the O^{2-} ions are *cis* and for Ti(2) they are in *trans* conformation. The Ti—O bonds opposite to the short bonds are quite long (2·09 and 2·15 Å). The short bonds are almost in the *ac* and *bc* planes respectively at an angle about 45° from the *c* axis. The Ti—O bonds perpendicular to the short bonds have atom to atom distances varying between 1·96 and 2·05 Å (bond distances resulting from the multipole refinements described below are given in Table 4). The titanium is displaced from the centre of its coordination octahedron. The average Ti—O distance is close to the value of 1·97 Å for rutile. An *ORTEP* (Johnson, 1965) plot showing the coordination of the titanium ions is given in Fig. 2.

Results

Table 2 gives agreement indices for the following models which have been iterated to convergence by a full-matrix least-squares refinement on F^2. The

Table 2. *Electron-density refinements*

Full data set: refinements of 5053 reflections. High order: refinements of 2440 high-order reflections ($\sin\theta/\lambda > 0.9$ Å^{-1}). See text for definitions of the KSph and KDef models. N_{var} is the number of parameters optimized by a full-matrix least-squares method.

	Free-atom full data set (FA)	Free-atom high order (FA-HO)	Multipole (KSph)	Multipole (KDef)
N_{var}	145	144	243	292
$R(F)$ (%)	1·86	2·46	1·67	1·42
$R(F^2)$ (%)	2·67	3·54	2·13	1·77
$wR(F^2)$ (%)	3·95	4·59	3·22	2·63
G.o.f.	1·84	1·29	1·51	1·24

results of four refinements are presented: a free-atom refinement of the full data set (FA), a similar refinement using only the high-order reflections having $\sin\theta/\lambda > 0.9$ Å^{-1} (FA–HO), then two aspherical atom models termed KSph and KDef corresponding to whether the nonspherically symmetric density functions were omitted or included for the potassium ions. There is no doubt about the statistical significance of the inclusion of density parameters into the atomic model. The differences in the structural parameters obtained from the refinements of the various models are only small. Coordinates from the refinement KDef are given in Table 3 and the corresponding interatomic distances in Table 4. The distances given here have been corrected for 'riding motion' (Busing & Levy, 1964), a correction which does not exceed 0·002 Å. They do not show large deviations from the earlier studies of

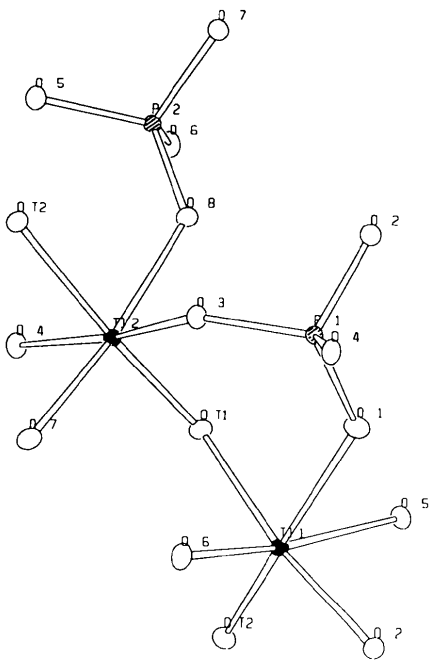

Fig. 2. *ORTEP* view (Johnson, 1965) of the coordination close to titanium.

Table 3. *Fractional coordinates* ($\times 10^6$) *and* U_{ij} *values* (Å$^2 \times 10^5$)

	x	y	z
Ti(1)	37293 (1)	50001 (2)	0
O(T2)	27623 (4)	54109 (9)	−11024 (5)
Ti(2)	24666 (1)	26941 (2)	25129 (2)
O(T1)	27529 (4)	46681 (8)	14324 (5)
P(1)	49805 (1)	33625 (2)	25987 (2)
O(1)	48570 (4)	48655 (8)	14995 (5)
O(2)	50992 (4)	46518 (9)	38292 (5)
O(3)	40031 (4)	19910 (8)	27915 (5)
O(4)	59353 (4)	19344 (8)	24046 (5)
P(2)	18083 (1)	50209 (3)	51241 (2)
O(5)	11248 (4)	31096 (8)	54089 (5)
O(6)	11145 (4)	69164 (8)	48694 (5)
O(7)	25276 (4)	53953 (8)	62766 (5)
O(8)	25294 (4)	46089 (9)	39915 (5)
K(1)	37709 (6)	77988 (7)	31023 (8)
K(2)	10569 (4)	70040 (10)	6486 (8)

	U_{11}	U_{22}	U_{33}	U_{12}	U_{13}	U_{23}
Ti(1)	493 (3)	453 (3)	426 (3)	−13 (3)	−27 (3)	61 (3)
O(T2)	825 (16)	824 (16)	747 (15)	−67 (14)	−292 (13)	170 (13)
Ti(2)	453 (3)	501 (3)	402 (3)	−27 (3)	51 (3)	−12 (3)
O(T1)	755 (16)	789 (16)	688 (15)	39 (13)	207 (12)	228 (13)
P(1)	367 (4)	538 (5)	478 (5)	−4 (4)	−68 (4)	24 (4)
O(1)	822 (15)	963 (17)	786 (14)	−150 (13)	−209 (12)	388 (13)
O(2)	766 (15)	1018 (16)	767 (15)	132 (13)	−268 (12)	−324 (13)
O(3)	443 (13)	754 (14)	959 (15)	−117 (11)	27 (11)	105 (12)
O(4)	442 (12)	866 (14)	1094 (17)	140 (11)	10 (11)	−91 (13)
P(2)	614 (5)	390 (4)	435 (5)	−27 (4)	33 (4)	−65 (4)
O(5)	910 (15)	464 (13)	955 (16)	−134 (12)	208 (12)	3 (11)
O(6)	1054 (16)	473 (13)	1123 (18)	134 (12)	−218 (13)	21 (12)
O(7)	947 (16)	891 (16)	707 (14)	203 (14)	−270 (13)	−336 (12)
O(8)	1007 (17)	959 (16)	675 (14)	−263 (14)	339 (12)	−331 (12)
K(1)	2266 (18)	1028 (13)	2024 (18)	433 (15)	551 (17)	104 (14)
K(2)	1264 (15)	2047 (19)	2338 (20)	516 (14)	−16 (16)	−141 (19)

Table 4. *Bond-vibration analysis*

Z^2 is the squared amplitude in the bond direction (A—B) and ΔZ^2 the difference for the atom pair. $\langle X^2 \rangle$ is the mean-square amplitude perpendicular to the bond. The bond length has been corrected for riding motion (Busing & Levy, 1964).

Atom A	Atom B	Z^2_A	Z^2_B	ΔZ^2	$\langle X^2_A \rangle$	$\langle X^2_B \rangle$	Corrected length (Å)
Ti(1)	O(T2)	0·0042	0·0048	0·0006	0·0047	0·0096	1·724
Ti(1)	O(2)	0·0048	0·0049	0·0001	0·0045	0·0103	1·962
Ti(1)	O(T1)	0·0047	0·0048	0·0001	0·0045	0·0087	1·979
Ti(1)	O(6)	0·0046	0·0051	0·0004	0·0045	0·0107	1·992
Ti(1)	O(5)	0·0047	0·0051	0·0003	0·0045	0·0091	2·048
Ti(1)	O(1)	0·0043	0·0058	0·0015	0·0047	0·0100	2·150
Ti(2)	O(T1)	0·0045	0·0048	0·0004	0·0046	0·0088	1·745
Ti(2)	O(7)	0·0045	0·0048	0·0003	0·0046	0·0103	1·972
Ti(2)	O(4)	0·0047	0·0048	0·0002	0·0045	0·0096	1·982
Ti(2)	O(8)	0·0043	0·0047	0·0004	0·0046	0·0109	1·992
Ti(2)	O(3)	0·0048	0·0052	0·0004	0·0044	0·0082	2·043
Ti(2)	O(T2)	0·0045	0·0058	0·0013	0·0045	0·0091	2·093
P(1)	O(1)	0·0047	0·0047	0·0000	0·0046	0·0105	1·521
P(1)	O(2)	0·0050	0·0052	0·0001	0·0044	0·0102	1·552
P(1)	O(3)	0·0043	0·0042	−0·0001	0·0048	0·0087	1·545
P(1)	O(4)	0·0045	0·0045	0·0000	0·0047	0·0097	1·543
P(2)	O(5)	0·0045	0·0046	0·0000	0·0049	0·0094	1·537
P(2)	O(6)	0·0052	0·0051	−0·0000	0·0046	0·0107	1·531
P(2)	O(7)	0·0051	0·0050	−0·0001	0·0047	0·0102	1·550
P(2)	O(8)	0·0046	0·0045	−0·0001	0·0049	0·0110	1·539

the structure of KTP, and the agreement with the study of Voloshina *et al.* (1985) is excellent, bond distances agreeing within the standard deviations (about 0·001 Å).

For both of the multipole refinements, the effect of the electroneutrality constraint is considerable. The program estimates that about 13 electrons would be

added if this constraint were released; most of the electrons would be allocated to the 4*s* states of the titanium ions (there are 80 valence electrons in the asymmetric unit) and the error sum would be decreased from 7362 to about 7060 (for the KDef model, but similar values are found for the KSph model). This improvement, affecting mainly the low-order reflections, is highly significant in statistical terms, but physically unsatisfactory. Thus, the electroneutrality constraint was maintained.

Comparison of refinements without and with multipole functions on the potassium ions

The scale factors from the refinements KDef and KSph differ by 0·3%. The residual density around the K^+ ions is more than halved upon inclusion of nonspherical multipole functions at these sites: from above 1 to about 0·4 e $Å^{-3}$ at the maximum (Fig. 3) – this improvement is highly significant. We attempted to use a Gram–Charlier expansion

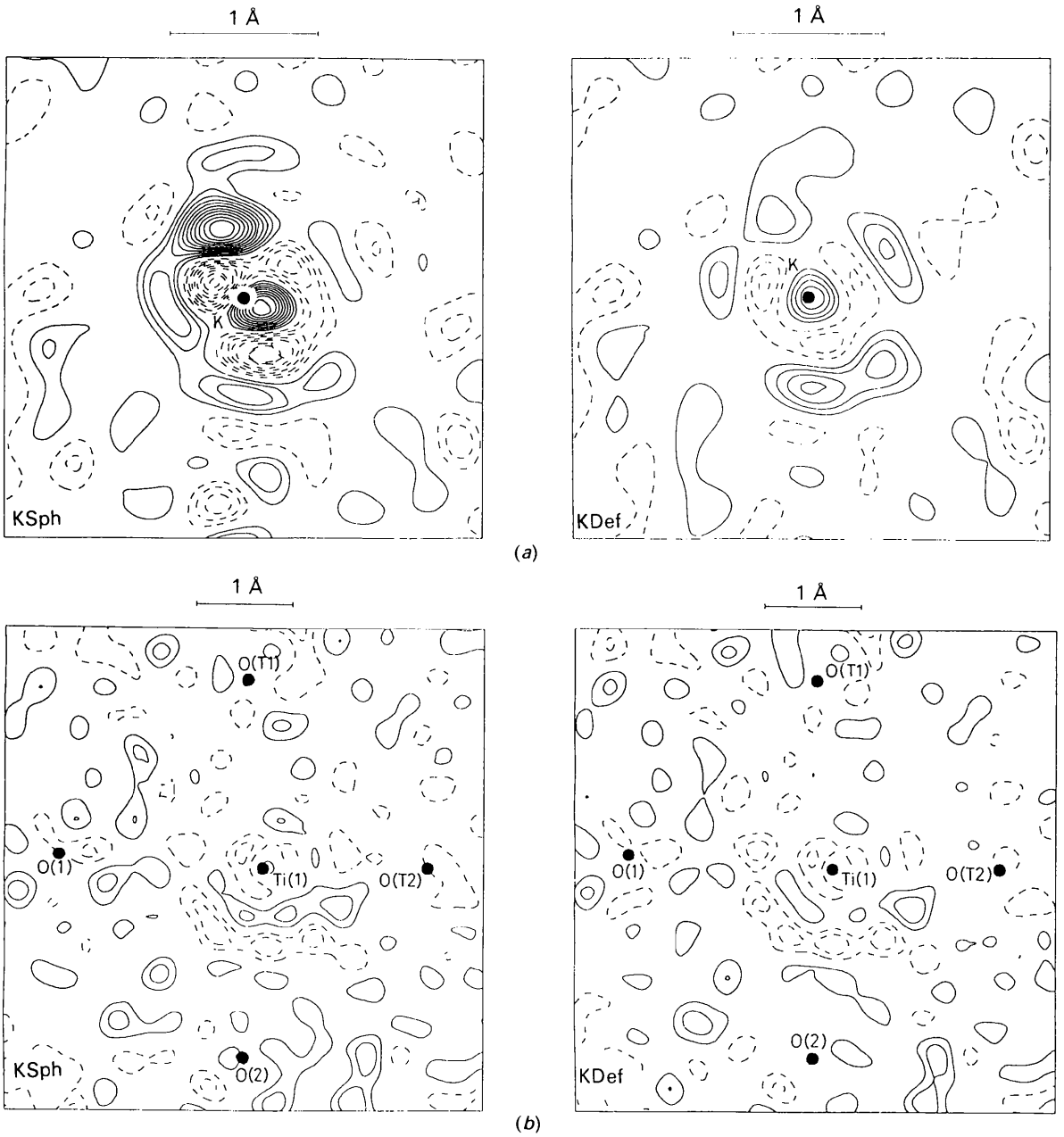

Fig. 3. Residual density maps at (*a*) K(1) and (*b*) Ti(1) for the refinements KSph and KDef. Interval between contours 0·1 e $Å^{-3}$ with broken contours for negative density and continuous for positive. The zero contour is omitted.

through to the sixth order of the potassium Debye–Waller factors (see for example Kuhs, 1983); the refinements were carried out with the *PROMETHEUS* program system (Zucker, Perenthaler, Kuhs, Bachmann & Schulz, 1983), but surprisingly this did not bring about any significant improvement of fit. For each refinement the residual features at the two independent potassium sites are similar indicating that they are not due to random errors. No large differences in the residual density were observed in other regions of the unit cell when comparing the two models (KDef and KSph); but in the neighbourhood of the titanium ions the *X–M* deformation density is sensitive to the treatment of the potassium ions (Fig. 4). At first sight these observations may seem contradictory. They may nevertheless be explained by the fact that two sets of model structure factors, differing mainly in their phases, will lead to rather similar values of $\Delta F_{\rm res} = [\,F_{\rm obs}(\mathbf{H}) - |F_{\rm model}(\mathbf{H})|] \times \exp(i\alpha_{\rm model})$, whereas $\Delta F_{\rm dyn} = F_{\rm obs}(\mathbf{H}) \exp(i\alpha_{\rm model})$

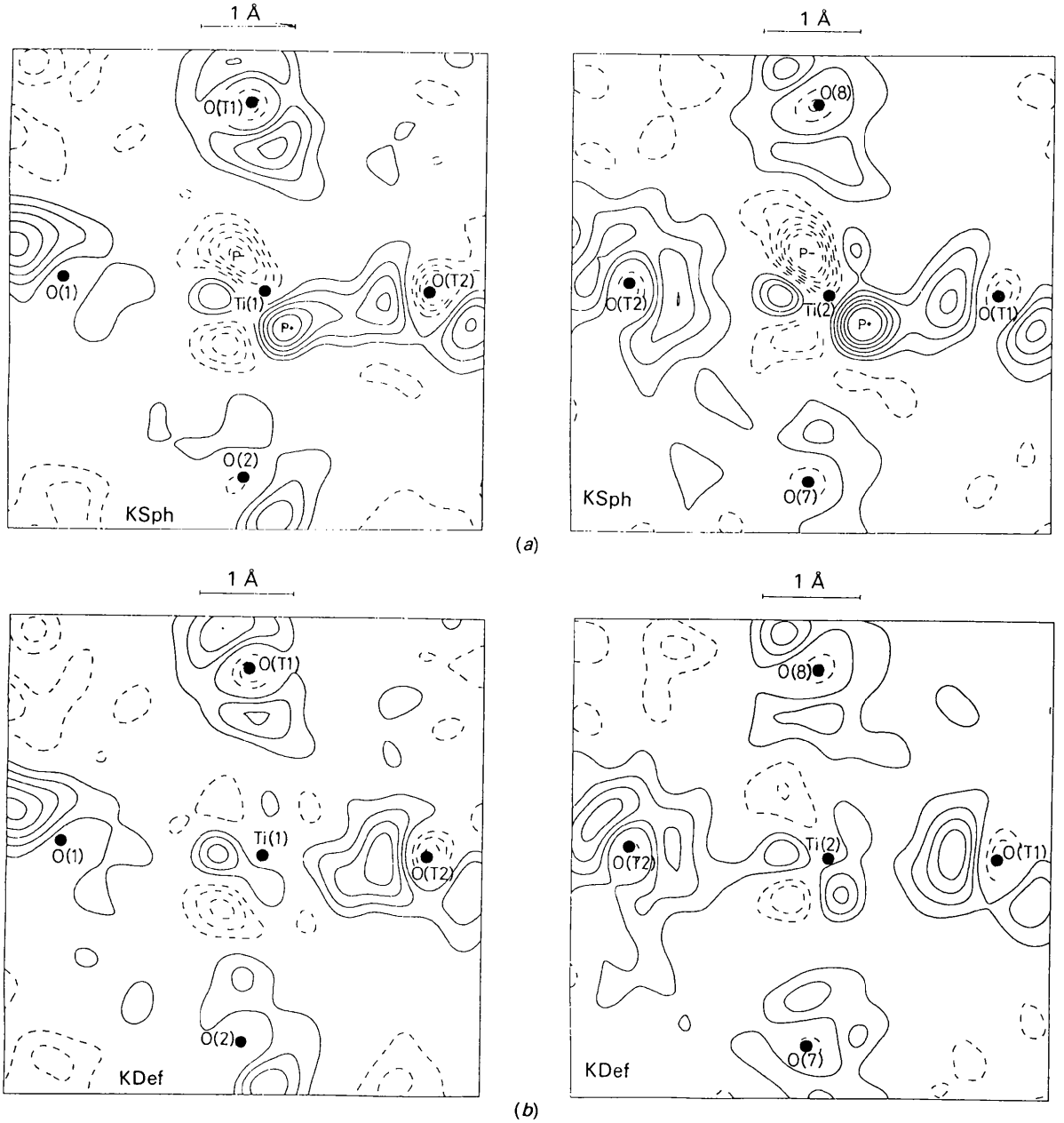

Fig. 4. *X–M* deformation-density maps at Ti(1) and Ti(2) for the refinements (*a*) KSph and (*b*) KDef. In all maps of these sections the short Ti—O bond is to the right. Contours as in Fig. 3.

$-F_{FA}(\mathbf{H})$ may show dramatic changes in both modulus and phase. This can be demonstrated in a fashion similar to the one used by Coppens for X–N densities for noncentrosymmetric structures (Coppens, 1974, Figs. 4 and 5.). The deformations observed in the X–M map (Fig. 4*a*) obtained using the KSph model do not correspond to next neighbour Ti—O interactions, the most prominent feature being 'dipole-like' and oriented parallel to the crystallographic c axis (*i.e.* on the diagonal of the section shown, indicated by P$^+$ and P$^-$), whereas when calculating the X–M density map using the phases of the KDef model, this feature almost disappears (Fig. 4*b*). It should be remembered that the X–M maps are affected by our rejection of the weakest and strongest reflections; nevertheless the static deformation maps, which are not directly affected by this rejection of reflections, show clearly the same features as the X–M maps (the results of the KDef refinement are given in Fig. 5). What manifests itself here is the fact that when the structure is noncentrosymmetric, the refinement of structure-factor moduli cannot be thought of as a refinement in positional space, because of the phase problem – modifying the description in one region of space leads to modifications all over – here we are touching on a problem already discussed by Nelmes & Tun (1987) and Hansen (1988). This is contrary to refinements of centrosymmetric structures, for which the proper signs of the structure factors may be predicted even with quite primitive models. The conclusion is that, for noncentrosymmetric structures, a model is needed which exhausts the information content in the data, but with the condition that the model must also be physically reasonable since parts of the electron density and the atomic positional probability density functions only affect the diffraction data by a minimal amount or not at all (see also Hazell & Willis, 1978). This we have not quite obtained, since we have not been able to explain the origin of the features which we, by our treatment (the KDef model), have located at the potassium sites.

Agreement between the best model (KDef) structure factors and observations

The distribution of normalized deviations $\Delta_N = (F^2_{obs} - F^2_{calc})/\sigma(F^2)$ (not shown) is, as the 'goodness of fit' parameter also indicates, broader than a normalized Gaussian. The distribution is slightly skewed with an excess of deviations greater than + 2.

The mean and the root-mean-square values of Δ_N (averaged over groups of 100 reflections) as a function of $\sin\theta/\lambda$ show a relatively good fit in the interval from 0·5 to 0·9 Å^{-1} (Fig. 6). Outside this interval the observed intensities are larger than the calculated ones. An even clearer trend is found when looking at these indicators as a function of the structure-factor modulus. Weak reflections are systematically observed stronger than predicted by the multipole model. This may well be a defect of the treatment of the measured profiles. It was noted that such a tendency was not observed when comparing hkl and $hk\bar{l}$ reflections, or when comparing the two data sets; on the other hand the comparison of the

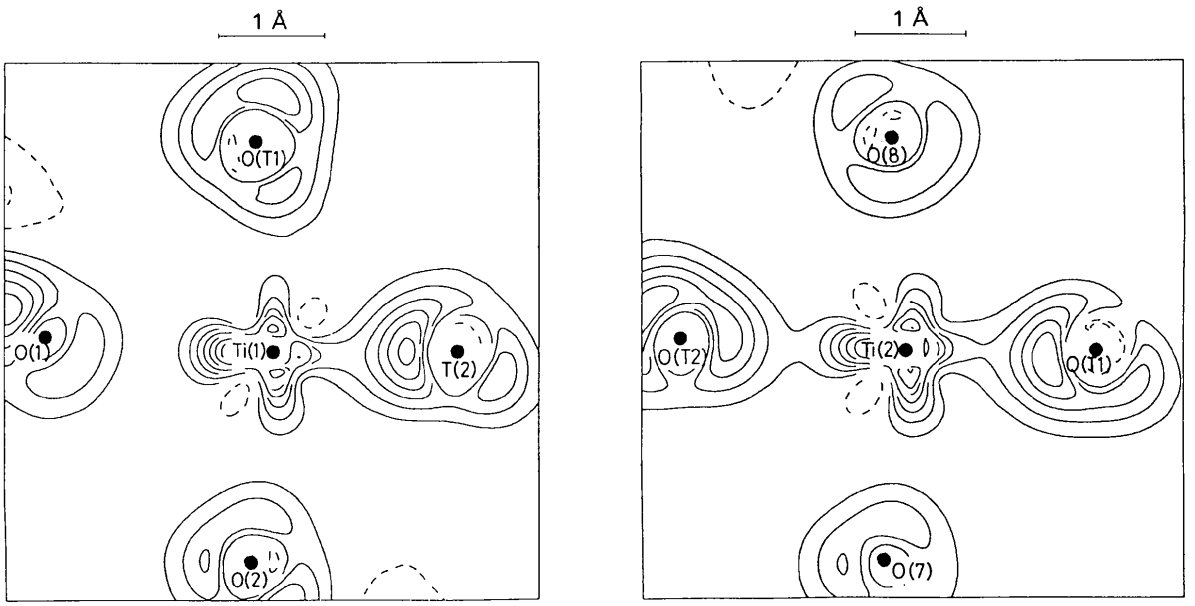

Fig. 5. Static deformation density based on the refinement KDef. The same sections through Ti(1) and Ti(2) as in Fig. 4. Contours as in Fig. 3.

internal agreements of the data sets indicated that the standard deviations of weak reflections are somewhat underestimated when proceeding as we have done. Nevertheless, these effects are not very important; the root-mean-square value for the full data set is inferior to 1·5, except for the very strongest reflections which are affected by secondary extinction.

Structure and thermal vibrations

The atomic displacement tensors have been used for calculating the mean-square amplitudes of vibration in the directions of the neighbouring atoms with the aim of estimating the strength of the interactions (see for example Hirshfeld, 1976). A compilation of differences, Δz^2, of mean-square amplitudes for pairs of atoms are given in Table 4. The mean-square amplitudes perpendicular to the bonds as well as bond distances corrected for riding motion are also reported (this correction only has a meaning for bonds where Δz^2 is small). For the phosphate-group bonds, values of Δz^2 are all smaller than 10^{-4} Å^2 (this deviation from zero is not statistically significant). Perpendicular to the bonds the oxygen amplitudes are about one and a half times that of the phosphorus atom. The same observation is made for the Ti—O pairs: the oxygen amplitudes in the bond direction are only very much larger than those of the titanium ions for the pairs separated by 2·15 and 2·09 Å. This analysis only gives a crude account of the strength of the bonding; the rigid-bond test is not sensitive enough to distinguish the strength of the short from the intermediate distances of the Ti—O interactions; but even the short Ti—O bonds are definitely less rigid than the P—O bonds.

Table 5. *κ values, valence populations and net charges with e.s.d.'s in parentheses*

	$\kappa(3d)$	P_{3d}	$P_{4s}(\kappa = 1)$
Ti(1)	1·13 (2)	1·89 (7)	0·2 (3)
Ti(2)	1·13 (2)	1·93 (6)	0·0 (3)
	κ	P_v	
O(T1)	0·941 (3)	7·12 (6)	
O(T2)	0·941 (3)	7·12 (6)	
P	1·10 (1)	4·27 (12)	
O(phosphate)	0·962 (2)	6·65 (04)	
Net charge Q (PO_4)		−1·85 (17)	

The effect of the titanium coordination on the phosphate-group oxygens is noted; *e.g.* the distance P(1)—O(1) is the shortest, the distance Ti(1)—O(1) is extremely long. We have nevertheless not attempted to take these differences into account in our electron-density modelling (by relieving the constraint of identical multipole expansions for all P—O bonds) since the residual density is low in the regions of the phosphate groups.

It may be noted that the amplitudes of atomic vibration, with the exception of the potassium ions, are quite small. Actually the independent-atom Debye temperatures are higher than room temperature for all of the atoms but the potassiums (unpublished results).

Atomic charges

The monopole populations, P_V, resulting from the refinement of the KDef model are listed in Table 5. It should be recalled that two constraints have been applied to these parameters: the unit cell is neutral and the valence populations of the potassium ions are kept fixed at $P_V = 0$.

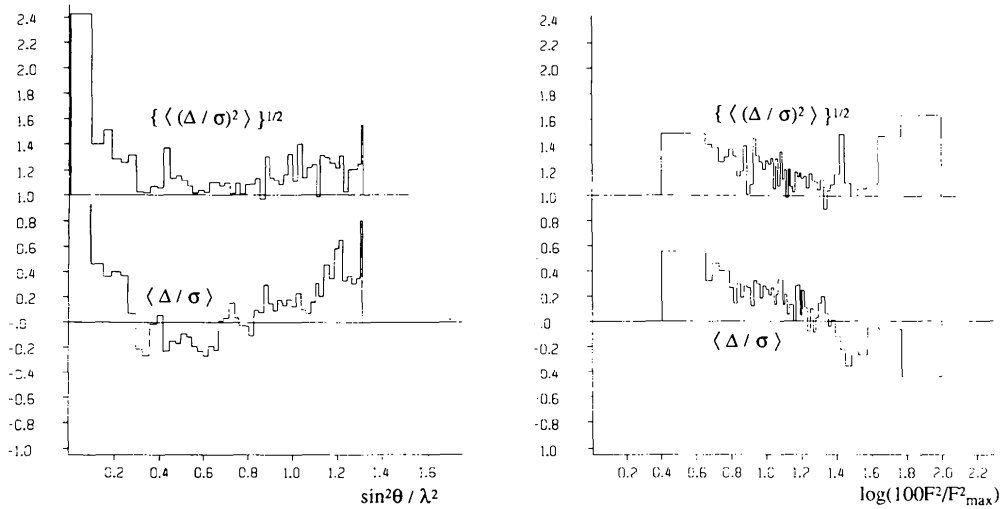

Fig. 6. Weighted deviates $\Delta = F^2_{obs} - F^2_{calc}(KDef)/\sigma(F^2)$ and their root-mean-square values as a function of $\sin\theta/\lambda$ and F. The block diagram shows averages over groups of 100 reflections.

The number of 3*d*-like electrons for titanium is only slightly below the free-atom value of two, and their distribution in space is more compact ($\kappa > 1$); the 4*s* populations show insignificant deviations from zero. This model is quite far from the expectations based on the formal charge of +4, *i.e.* $P_V(3d) = 0$, but this may be due to the covalent character of the oxotitanium bond. The valence populations of oxygen ions (corresponding to an approximate atomic charge of −1) agree with this idea. It is noted that the crystallographically independent ions turn out to have very similar charges.

The populations of the phosphorus and the oxygen atoms belonging to the phosphate group are rather strongly correlated ($\gamma = 0{\cdot}74$). The net charge of the group (−1·85) is smaller than its formal charge (−3). It has often been observed that analysis of the electron-density distribution in terms of charges leads to values closer to neutral than predicted by ionic models.

Electron-density distribution

The residual maps show no systematic features, apart from the K^+ region. The maximum absolute value found in the calculated planes is about 0·2 e Å $^{-3}$. As estimates of random error in the total electron density $\frac{1}{V}\{\sum\sigma^2[F(\mathbf{h})]\}^{1/2}$ and $\frac{1}{V}\{\sum[\Delta F(\mathbf{h})]^2\}^{1/2}$ may be used (the summations extend over a full sphere of data), which for our data are set equal to 0·07 and 0·13 e Å $^{-3}$ respectively. Owing to this noise level we represent the densities as maps with an interval of 0·1 e Å $^{-3}$ between contours (the zero contour is omitted).

As pointed out by Coppens & Stevens (1977), one can take into account the effect of random errors but

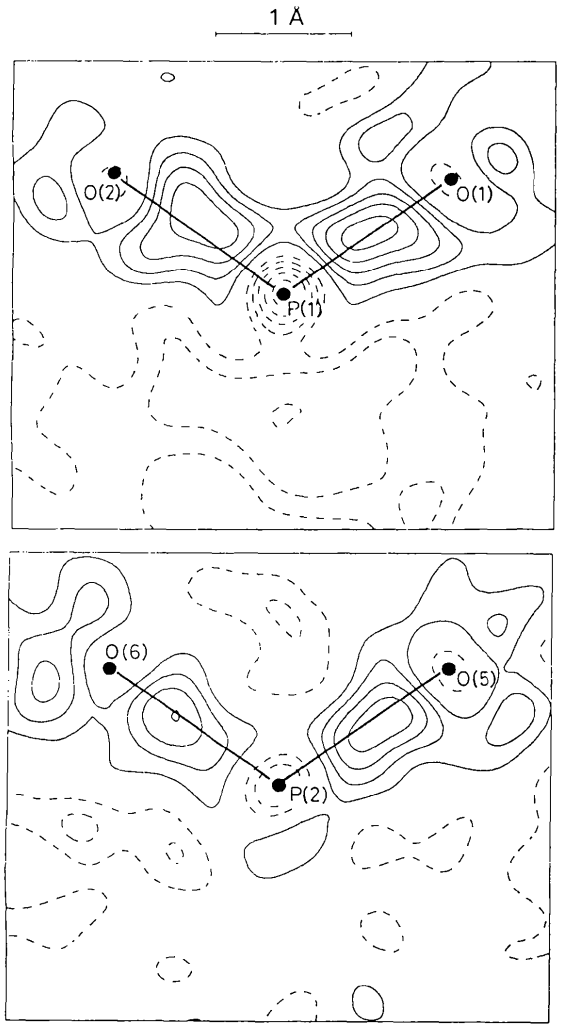

Fig. 7. *X*–*M* deformation-density maps of two PO_2 segments. Contours as in Fig. 3.

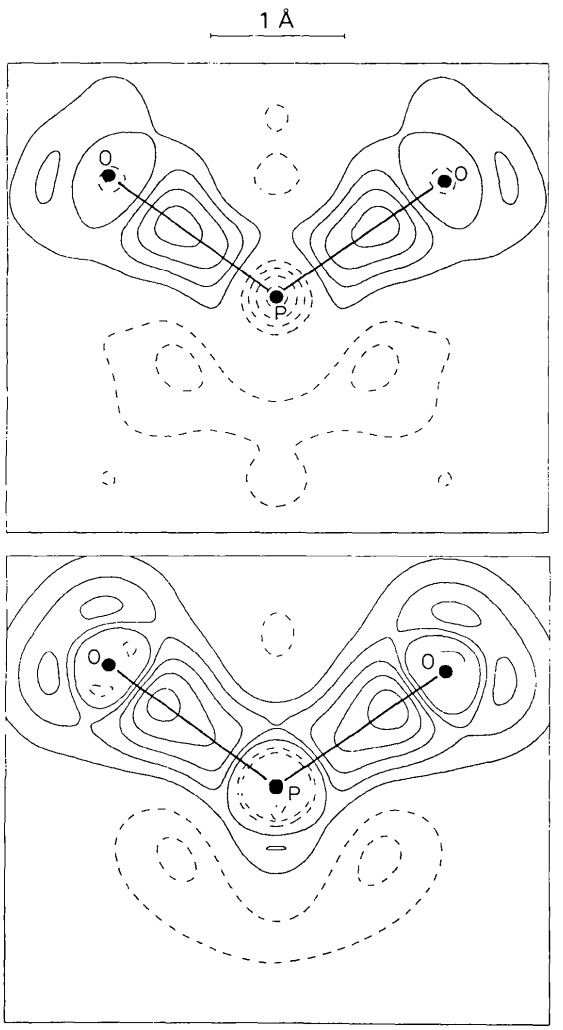

Fig. 8. Averaged *X*–*M* and static deformation-density maps for the PO_2 segment. Contours as in Fig. 3.

not readily systematic errors in the thermal-motion model: in the present case we are limited to anisotropic harmonic motions. Nevertheless, the thermal-vibration amplitudes are quite small, so the static maps show only slightly higher densities than the dynamic maps in regions away from the atomic nuclei [outside a radius of about 0·3 Å which corresponds to the resolution for $\sin(\theta)/\lambda < 0{\cdot}9$ Å^{-1}]. We therefore estimate that the random errors in the extranuclear regions of the static maps are of the order of 0·1 e Å^{-3}.

The phosphate groups

We shall first take a look at the deformation density of the phosphate groups. We are not aware of any reliable experimental electron-density study of phosphate-containing compounds. The group must be considered as having definite covalent bonds and a theoretical calculation of the deformation density in H_3PO_4 with which comparisons can be made has been published by Blessing (1988): an SCF wavefunction of split-valence plus polarization quality equivalent to 6-31G** (Moss & Blessing, 1984). In Fig. 7 *X–M* deformation maps are shown in two independent sections [P(1)—O(1)—O(2) and P(2)—O(3)—O(4)], and in Fig. 8 a density map is shown which is the mean of four such planes and which has been further averaged about the bisector of the O—P—O angle. This figure also shows a static deformation density which perfectly reproduces the *X–M* map with only a small expected increase of the extreme values of the density. The rather severe constraints which have been imposed on the phosphate-ion density do not explicitly allow for deformations due to an interaction with the Ti^{4+}. Nevertheless the residual densities (not shown) indicate that the model is sufficiently flexible. The deformation density of the phosphate ion seems quite reasonable, the excess density in the bond is almost identical to the value found by Blessing (1988) for the P=O bond in the phosphoric acid molecule. Lone-pair density is observed, but stronger and more localized in theory than experiment; this may to a large extent be due to a choice of too diffuse radial functions for the multipole expansion. With our restricted model, a compromise must be made when describing a rather localized lone-pair density and at the same time a more delocalized contribution from bond orbitals. With these limitations in mind we consider the agreement between theory and experiment altogether satisfactory.

We only know of one other experimental study of a phosphate-containing compound: $AlPO_4$ (Ngo-Thong & Schwarzenbach, 1979) for which the bonding is quite different from KTP. The agreement with our results is not very close; they find that all bonds are bent, P—O as well Al—O, and it is hard to distinguish phosphorus from aluminium due to the symmetry of the structure; $AlPO_4$ is a homeotype of α-quartz.

The Ti—O *coordination octahedra*

Our major interest is in the deformation density around the two crystallographically independent

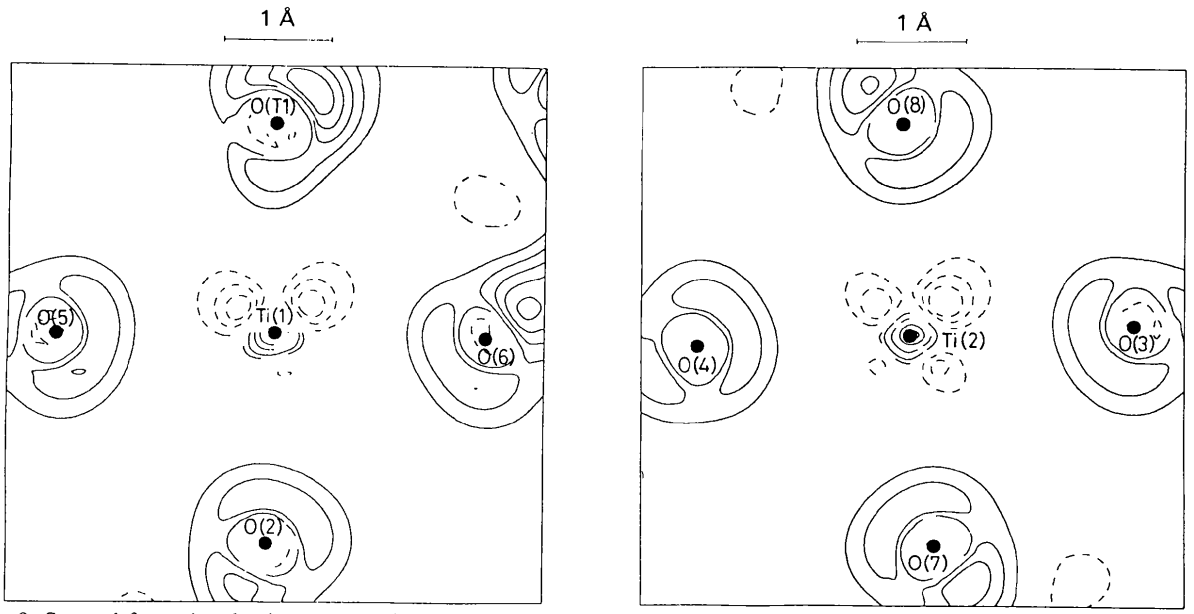

Fig. 9. Static deformation-density map, sections perpendicular to the short Ti—O bonds and passing through the titanium ions. Contours as in Fig. 3.

oxotitanium groups. The residual maps (Fig. 3) show two annular regions of predominantly positive and negative density around the titanium ions, but they do not exceed 0·25 e $Å^{-3}$ which is not higher than observed in regions further away from the atoms. The residual density seems to be completely random close to oxygen ions. The resemblance of the *X–M* maps for the sections through the two titanium ions (Fig. 4) is striking. They have all the major features in common such as the positive deformation in the short Ti—O bond peaking at a distance of 0·45 Å from the oxygen-nuclear position. This peak is also at a distance corresponding to the maximum of the 4*s* orbital for the free titanium atoms [r_{max} = 1·32 Å for a single Slater-type orbital (Clementi & Raimondi, 1963)]. Weak lone-pair electron densities are found at the other oxygen ions. In the vicinity of the titanium ions the prominent feature is the maximum surrounded by a negative region and placed in the direction of the more distant oxygen ion, but we still suspect that these features are to a large extent related to the residual density at the potassium sites.

The static deformation maps reproduce the same features. The oxygen lone-pair maxima are increased by about 20% whereas the density around the titanium ions shows a much larger enhancement. This is explained by our use of quite sharp radial functions for titanium, and the differences between *X–M* and static maps are to a large extent due to the limited resolution of the Fourier maps. As we did not refine the value of κ' for either titanium or oxygen, we cannot interpret the distances of the extrema from the nuclei observed in the static maps, but the model allows for full freedom of angular variation which is only limited by the expansion length, $l \leq 4$ (equations 1*a* and 1*b*). The density distribution in the Ti(2) octahedron has a nearly fourfold symmetry (Fig. 9). For Ti(1) this is not the case. The difference is explained by the *trans* conformation of the two O^{2-} ions with respect to Ti(2), whereas the conformation is *cis* for Ti(1).

The densities between the ions in the two short Ti—O bonds are alike, the differences can hardly be considered significant. We have taken a closer look at the positions of the maxima near the O^{2-} ions (maps not shown). Each ion is coordinated by the two titanium ions, two maxima are found in the direction of these ions and no other significant features are observed in the vicinity of the oxygen ions. The deformation density in the shorter Ti—O bonds is about one and a half times higher than in the long bonds.

Comparison with other diffraction studies

We can compare our results with the study carried out by Voloshina *et al.* (1985) for KTP. They presented Fourier maps of the thermally smeared deformation density. In their least-squares analysis, deformations in the P—O bonds were taken into account by placing additional scattering centres in these regions. In reasonable agreement with the present work, they found an excess density ranging from 0·3 to 0·6 e $Å^{-3}$ at the midpoint of these bonds, but they did not find any notable deformation within the titanium coordination octahedra ($\Delta\rho$ < 0·2 e $Å^{-3}$). Very large negative deformation densities are found centred at all atomic positions.

Our deformation density in the TiO_4 sections may be compared with results for rutile, TiO_2 (Restori, Schwarzenbach & Schneider, 1987). All the Ti—O bond lengths in rutile are close to 1·96 Å. The maxima in their static deformation density are at distances of about 0·6 Å from the oxygen ions with a peak value of around 0·3 e $Å^{-3}$. This is rather different from our observations for the Ti—O bonds in KTP, where the peaks are closer to the O^{2-} ions and higher.

Concluding remarks

We have obtained a consistent picture of the electron-density distribution in KTP in the sense that we find the same features for crystallographically independent, but chemically similar groups. Of special interest are the short Ti—O bonds for which we find a much more pronounced excess electron density than for the other bonds. The phosphate to titanium interactions seem to be of an electrostatic nature. This observation agrees perfectly with our discussion of the nonlinear optical properties (Hansen, Protas & Marnier, 1988). The nonlinearity of KTP can be explained by the hyperpolarizability of the short Ti—O bonds, and accordance with the idea that the hyperpolarizabilities are largest for polar covalent bonds. We may also remark that this is the first experimental study which gives a high-quality electron-density distribution of a phosphate group. Temperature-dependent X-ray diffraction measurements have been undertaken; the results will be presented with a detailed discussion of the probability distribution of the potassium ions. A neutron diffraction analysis is also underway.

References

BECKER, P. & COPPENS, P. (1974). *Acta Cryst.* A**30**, 129–147.

BLESSING, R. H. (1987). *Crystallogr. Rev.* **1**, 3–58.

BLESSING, R. H. (1988). *Acta Cryst.* B**44**, 334–340.

BUSING, W. R. & LEVY, H. A. (1964). *Acta Cryst.* **17**, 142–146.

CLEMENTI, E. & RAIMONDI, D. L. (1963). *J. Chem. Phys.* **38**, 2686–2689.

CLEMENTI, E. & ROETTI, C. (1974). *At. Data Nucl. Data Tables*, **14**, 177–478.

COPPENS, P. (1974). *Acta Cryst.* B**30**, 255–261.

COPPENS, P. & STEVENS, E. D. (1977). *Isr. J. Chem.* **16**, 175–179.
HANSEN, N. K. (1988). *Acta Cryst.* A**44**, 1097.
HANSEN, N. K. & COPPENS, P. (1978). *Acta Cryst.* A**34**, 909–921.
HANSEN, N. K., PROTAS, J. & MARNIER, G. (1988). *C. R. Acad. Sci. Ser. B*, **307**, 475–478.
HAZELL, R. G. & WILLIS, B. T. M. (1978). *Acta Cryst.* A**34**, 809–811.
HIRSHFELD, F. L. (1976). *Acta Cryst.* A**32**, 239–244.
JOHNSON, C. K. (1965). *ORTEP*. Report ORNL-3794. Oak Ridge National Laboratory, Tennessee, USA.
KUHS, W. F. (1983). *Acta Cryst.* A**39**, 148–158.
LEVINE, B. F. (1973). *Phys. Rev. B*, **7**, 2600–2626.
MARNIER, G. (1988). US Patent, CNRS No. 4746396 (24 May 1988).
MOSS, G. R. & BLESSING, R. H. (1984). *Acta Cryst.* A**40**, C-157.
NELMES, R. J. & TUN, Z. (1987). *Acta Cryst.* A**43**, 635–638.
NGO THONG & SCHWARZENBACH, D. (1979). *Acta Cryst.* A**35**, 658–664.
RESTORI, R., SCHWARZENBACH, D. & SCHNEIDER, J. R. (1987). *Acta Cryst.* B**43**, 251–257.
ROGERS, D. (1981). *Acta Cryst.* A**37**, 734–741.
SASAKI, S. (1984). *Anomalous Scattering Factors for Synchrotron Radiation Users Calculated using the Cromer–Liberman's Method*. Internal Report. National Laboratory for High Energy Physics, Oho-machi, Tsukuba-gun, Ibaraki-ken 305, Japan.
STUCKY, G. D., PHILLIPS, M. L. F. & GIER, T. E. (1989). *Chem. Mater.* **1**, 492–509.
THOMAS, P. A., GLAZER, A. M. & WATTS, B. E. (1990). *Acta Cryst.* B**46**, 333–343.
TORDJMAN, I., MASSE, R. & GUITEL, J. C. (1974). *Z. Kristallogr.* **139**, 103–115.
TSIREL'SON, V. G., KOROL'KOVA, O. V. & OZEROV, R. P. (1984). *Sov. Phys. Crystallogr.* **29**, 1–4.
VOLOSHINA, I. V., GERR, R. G., ANTIPIN, M. YU., TSIREL'SON, V. G., PAVLOVA, N. I., STRUCHKOV, YU. T., OZEROV, R. P. & REZ, I. S. (1985). *Sov. Phys. Crystallogr.* **30**, 389–393.
ZUCKER, U. H., PERENTHALER, E., KUHS, W. F., BACHMANN, R. & SCHULZ, H. (1983). *J. Appl. Cryst.* **16**, 358.
ZUMSTEG, F. C., BIERLEIN, J. D. & GIER, T. E. (1976). *J. Appl. Phys.* **47**, 4980–4985.

Acta Cryst. (1991). B**47**, 672–678

Structural Changes in O′-Sialons, $Si_{2-x}Al_xN_{2-x}O_{1+x}$, $0{\cdot}04 \le x \le 0{\cdot}40$

BY O. LINDQVIST AND J. SJÖBERG*

Department of Inorganic Chemistry, Chalmers University of Technology and University of Göteborg, S-412 96 Göteborg, Sweden

S. HULL

ISIS Science Division, Rutherford–Appleton Laboratory, Chilton, Didcot, Oxon OX11 0QX, England

AND R. POMPE

Swedish Ceramic Institute, Box 5403, S-402 29 Göteborg, Sweden

(*Received* 15 *February* 1991; *accepted* 22 *April* 1991)

Abstract

Structural changes in the aluminium silicon nitride oxide $Si_{2-x}Al_xN_{2-x}O_{1+x}$, O′-sialon, due to gradually varying stoichiometry, have been studied by Rietveld analysis of time-of-flight powder diffraction data from a pulsed neutron source. Refinements were based on the orthorhombic space group $Cmc2_1$ with cell dimensions, depending on composition, in the ranges $a = 8{\cdot}8807\ (13)$–$8{\cdot}9254\ (5)$, $b = 5{\cdot}4965\ (4)$–$5{\cdot}4988\ (7)$ and $c = 4{\cdot}8550\ (6)$–$4{\cdot}8596\ (2)$ Å. $V = 237{\cdot}00\ (6)$–$238{\cdot}45\ (2)$ Å^3, $Z = 4$, $D_x = 2{\cdot}81\ (1)$ g cm^{-3}, $M_r = 100{\cdot}22$–$100{\cdot}54$. Neutrons with time-of-flight from 2000 to 20000 μs for a total flight path of 12 m and detectors placed at 130–158° (2θ), averaged to 145°, were used for data acquisition at room temperature under vacuum ($< 10^{-4}$ Pa). Final R_I values (for intensities) vary from 0·038 to 0·070 and R_p values (for profile) from 0·045 to 0·086. Only the (Si,Al)—O(2) bond length is significantly influenced by the change in composition, whereas the Si—O(2)—(Si,Al) bond angles, connecting the puckered layers of Si,Al and N,O(1), remains unchanged. The change in (Si,Al)—O(2) bond length is related to the change in occupancies of Si and Al in the tetrahedral site, *i.e.* to the change in x, and is in agreement with the expression $(1 - x/2)1{\cdot}62$ Å + $(x/2)1{\cdot}77$ Å, which has been determined for layered silicates. No ordering of the replacing atoms has been observed for the range of O′-sialons studied. The JCPDS File Nos. for the samples are: for $x = 0{\cdot}40$, No. 42-1490; for $x = 0{\cdot}16$, No. 42-1491; and for $x = 0{\cdot}04$, No. 42-1492.

* To whom correspondence should be addressed.

0108-7681/91/050672-07$03.00